Materials Horizons

COMMUNICATION

Plasmon-enhanced magneto-optical detection of single-molecule magnets

Received 00th January 20xx,
Accepted 00th January 20xx

DOI: 10.1039/x0xx00000x

www.rsc.org/

Francesco Pineider[a,b*], Esteban Pedrueza-Villalmanzo[c], Michele Serri[b§], Addis Mekonnen Adamu[c,d], Evgeniya Smetanina[c], Valentina Bonanni[b‖], Giulio Campo[b‡], Lorenzo Poggini[b], Matteo Mannini[b], César de Julián Fernández[e], Claudio Sangregorio[f], Massimo Gurioli[g], Alexandre Dmitriev[c], Roberta Sessoli[b]

Here we report on nanoarchitectures composed of molecular magnets on optical nanoantennas. We demonstrate a significantly boosted magneto-optical detection of a thin film of a Terbium(III) bis-phthalocianinato ($TbPc_2$) single-molecule magnet and we track down the origin of this enhancement to nanoantenna effects at the optical level. This finding suggests that the vast knowledge on plasmon-enhanced spectroscopies can be readily extended to magneto-optics, thus paving the way to strong magneto-optical enhancements for the readout of nanometric devices embedding single-molecule magnets.

Plasmonic nanoantennas deliver on their outstanding optical and electronic properties,[1-4] able of altering the local distribution of the electric[4] and magnetic fields[5] at optical frequencies. This makes them appealing as advanced sensors, hot-electron providers, and local heaters, to name a few. Subwavelength electromagnetic field confinement by plasmon nanoantennas allows identification of trace amounts of molecular compounds when combined with surface-enhanced Raman scattering,[6] plasmon-enhanced luminescence,[7] Brillouin scattering,[8] circular dichroism[9] and magneto-optical spectroscopy.[10-14] So far, despite several works reported on optical properties of molecular-plasmonic systems, there are no studies involving molecular magnets and plasmonic enhancement of their magneto-optical effects. The addition of a magnetic functionality to the molecular moiety introduces an extra degree of freedom that could be important for the fundamentals and applications in opto-magnetics[15] and in photonic-spintronic phenomena.[16] In this respect, molecular nanomagnets[17], with the richness of their chemical, electronic and magnetic properties, represent a versatile playground to explore new complex systems. These mono- and poly-nuclear transition metal or rare earth complexes have been proposed as nanoscopic memory units for next generation computing[18] and have been widely studied for quantum computation purposes down to the nanoscale.[19] Moreover, the semiconducting nature of some of these systems makes them promising candidate materials as spin valves in molecular spintronics.[20-23]

To fully exploit the potential of molecular nanomagnets, single molecules must be made accessible to addressing and manipulation by organization on different kinds of surfaces. Several device-oriented approaches to organize magnetic molecules have been proposed, from molecular self-assembly to physical vapor deposition.[24, 25] However, assembling magnetic molecules presents the additional challenge of the characterization of their physical properties. Whereas common magnetometric techniques fail to address monolayers and ultrathin films of single-molecule magnets, X-ray Magnetic Circular Dichroism (XMCD) has been successfully used to probe their magnetic properties.[26-28] This technique, however, has the disadvantage of being currently based on synchrotron radiation, thus with limited access.

To make this class of materials exploitable in devices, a readout approach must be devised that is at the same time highly sensitive and scalable to practical size. In this work, we propose a laboratory-scale method to study thin films of molecular nanomagnets, based on plasmon-enhanced magneto-optics. We deposited by thermal sublimation in high vacuum a ~2 nm layer of $TbPc_2$ (see Figure 1a for

[a] Department of Chemistry and Industrial Chemistry & INSTM, University of Pisa, Pisa, Italy.
[b] Department of Chemistry 'Ugo Schiff' & INSTM, University of Florence, Sesto Fiorentino (FI), Italy.
[c] Department of Physics, University of Gothenburg, Göteborg, Sweden.
[d] Department of Physics, Bahir Dar University, Bahir Dar, Ethiopia.
[e] CNR-IMEM, Parma, Italy.
[f] CNR-ICCOM, Florence, Italy.
[g] Department of Physics and Astronomy, University of Florence, Sesto Fiorentino (FI), Italy.
*francesco.pineider@unipi.it
§ Present address: Italian Institute of Technology, Genoa, Italy
‖ Present address: Department of Physics, University of Milan, Milan, Italy
‡ Present address: European Laboratory for Non-Linear Spectroscopy, University of Florence, Sesto Fiorentino (FI), Italy

Electronic Supplementary Information (ESI) available: Calculated absorption and scattering cross sections of nanodisks; calculated absorption and scattering cross sections; calculated near field maps; comparison of extinction of gold nanodisks with the real part of the dielectric function of TbPc2; fitting of optical spectra of $TbPc_2$ films on glass and on gold nanodisks; fitting of optical and magneto-optical spectra of gold nanodisks; optical spectra of $TbPc_2$ film on detuned gold nanodisks; field dependence of the magneto-optical signal of gold nanodisks; calibration curve for TbPc2 film thickness; AFM topography scan of gold nanodisks with TbPc2. Details on fitting procedures. Estimate of the limit of detection of TbPc2 with MCD. See DOI: 10.1039/x0xx00000x

molecular structure)[29] on an array of gold plasmonic nanoantennas, substantially enhancing the optical response from the $TbPc_2$. With magnetic circular dichroism (MCD) experiments we connected such enhancement to magneto-optics, thus allowing us to obtain spectroscopic and magnetometric information on reduced amounts of magnetic molecules on surface. To our knowledge, this is the first report of plasmon-enhanced magneto-optics carried out on molecules. Building on this solid proof of concept, we can anticipate that with further optimization of optical nanoantennas and deposition methods, plasmon-enhanced magneto-optical spectroscopy can reach record capabilities in the study of magnetic molecules.

$TbPc_2$ was chosen as a model single-molecule magnet system, due to the exciting results obtained when organized at the nanoscale[23, 24, 30-32] and because of the possibility of preparing ordered films on several types of substrate through thermal evaporation.[30, 31] In addition, $TbPc_2$ has a sharp optical resonance in the visible spectral range due to a strong π–π^* electronic transition of the phthalocyanine ligands, referred to as the Q band.[33] In $TbPc_2$ the Q band is strongly spin polarized due to hybridization with the frontier orbitals of terbium.[34] Due to this sharp, spin-polarized absorption, magneto-optical techniques are particularly suited for studying this molecular magnet.[31, 35-37]

The plasmonic gold nanodisks antennas with radius R = 62 nm and height h = 35 nm are produced on a glass substrate (filling fraction ~12%) by hole-mask colloidal lithography (Figure 1b).[38] Here nanoantennas are not covered by ligands, and a clean metallic surface is exposed for functionalization or physisorption. The process affords arrays of short-range-ordered nanostructures over cm^2 areas, with high flexibility of the geometric parameters of the nanostructures such as diameter, height, composition, etc.). By tuning aspect ratio and volume, this method allows control of the position of the localized surface plasmon resonance (LSPR) of the nanostructure with high precision over a wide energy range. In this size range the scattering contribution dominates over absorption (see cross sections calculated for a similar geometry in Figure S1, ESI, using the finite-difference time-domain, FDTD Lumerical software). Inter-particle distance is on average higher than twice the diameter of the disk, so collective LSPR phenomena are not fully negligible but do not play a significant role on the optical properties of the samples. Since no long-range order is present, diffractive contributions are absent. In this study, LSPR is nearly matching the strong absorption of the Q band of $TbPc_2$.

The molecular-plasmonic architecture is sketched in Figure 1c. A 2 nm layer of $TbPc_2$ was deposited on the nanoantennas using an established thermal sublimation method in high vacuum which allows the fabrication of high purity molecular films with an excellent degree of thickness control and high homogeneity over large areas.[30,32,39] The molecular layer covers the whole surface of the plasmonic substrate, including the areas between disks. A control sample was prepared by simultaneous deposition of $TbPc_2$ on a glass substrate without Au nanostructures (see ESI for details). Throughout the rest of the paper the pristine Au nanodisk sample will be identified as **AuDisks**, the layer of $TbPc_2$ as **$TbPc_2$**, and the 2 nm molecular deposit on the metallic nanostructure as **$TbPc_2$@Au**. All samples were studied by extinction spectroscopy at room temperature and MCD spectroscopy at 1.5 K in the visible/near-infrared energy range. Figure 2a shows the extinction of **AuDisks, $TbPc_2$** and **$TbPc_2$@Au**. The LSPR of **AuDisks** is at ~1.80 eV; the main resonance of **$TbPc_2$** is the sharp Q band at 1.85 eV,[40] which is the only resolved feature for this film thickness. The extinction spectrum of **$TbPc_2$@Au** shows a shift of LSPR of around 65 meV, from 1.80 to 1.73 eV, compared to the pristine nanoantennas. A shoulder on the high energy side of the plasmon resonance is clearly visible and ascribed to the Q band of $TbPc_2$. Compared to the same molecular deposit on bare glass (inset of Figure 2a), the extinction at resonance appears more intense (a detailed analysis is given in the discussion).

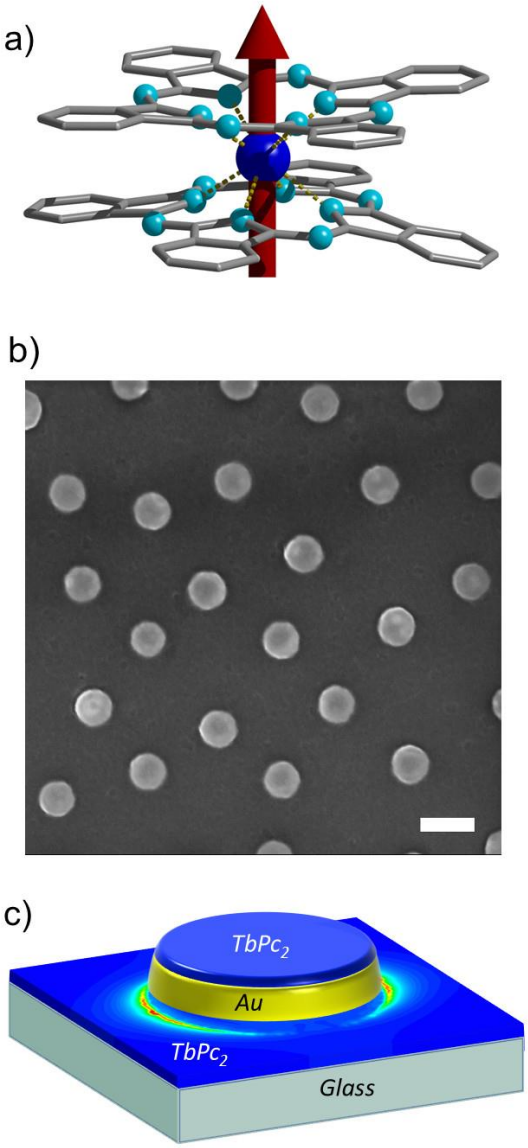

Figure 1. a) Structure of TbPc2 (red arrow: magnetic anisotropy axis); **b)** SEM image of the Au nanoantennas. Scale bar is 200 nm; **c)** Schematic representation of the TbPc2 layer on nanoantennas overlayed with finite-difference time-domain (FDTD) simulations of the electromagnetic near-field around the nanoantenna.

To support the experimental results, we performed FDTD simulations on a single, glass-supported gold nanodisk antenna with and without the $TbPc_2$ layer to analyze the far-field and the near- field responses of the system. The far field spectra calculated for a clean disk and a disk covered by a 2 nm layer of **$TbPc_2$** are reported in Figure 2b.

Optical constants for $TbPc_2$ were taken from an experimental ellipsometric study by Robaschik et al.;[31] details on the calculation can be found in the ESI. The calculations capture reasonably well the behavior of both the nanoantenna and the enhancement in the extinction of the $TbPc_2$ layer, as compared to the same layer on bare glass. We note that the near-field of the nanoantenna does not noticeably change by the addition of the thin $TbPc_2$ layer (Figure S2, ESI).

As mentioned above, several reports showed that molecular and plasmonic resonances which are spatially and energetically overlapping can undergo strong coupling resulting in mode hybridization,[41-44] or can exhibit interference effects (i.e. weak coupling regime), resulting in Fano-like line shapes of the molecular exciton.[45-47] The distinction between the two regimes is not always straightforward nearby the onset of the transition between strong coupling and weak coupling, i.e. near the exceptional point[48, 49]. The complexity in assessing the light matter interaction regime is even more intricated in our case, taking into account the magnetic response of both plasmonic and excitonic resonances. Still in both strong coupling and weak coupling regimes, we do expect similar results in terms of plasmonic enhancement of magneto-optics. Here we focus the attention on plasmon-enhancement effects in molecular magneto-optics and we describe the composite system by a weak coupling regime both in optics and magneto-optics. We can thus perform a deconvolution of the experimental data assuming a linear combination of nanoantenna resonance and the molecular

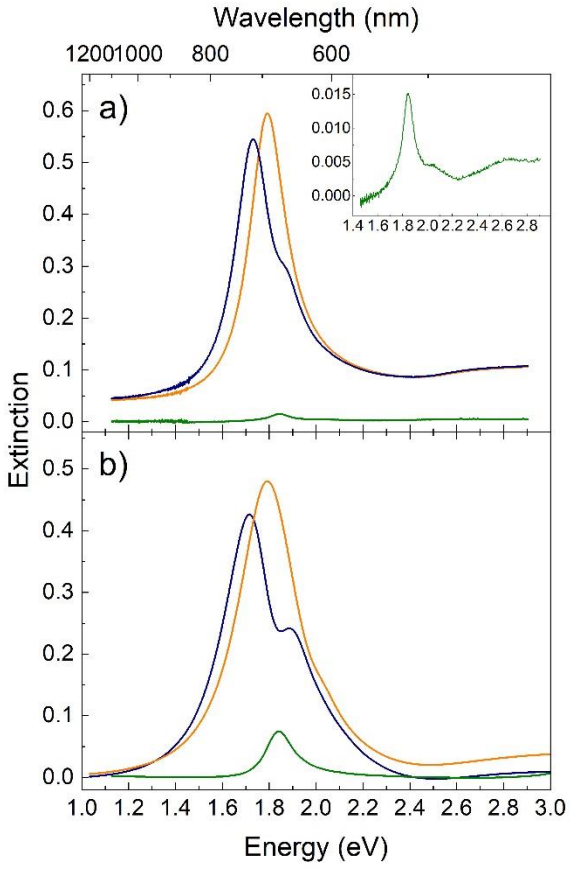

Figure 2. a) Experimental extinction spectra of **AuDisks** (orange), **$TbPc_2$** (green) and **$TbPc_2$@Au** (blue). Inset shows the enlarged Q band of TbPc2; same units as the main panel. **b)** Calculated far-field extinction of the same systems.

absorption to the optical extinction. Nanoantenna LSPR undergoes a 60 meV shift upon deposition of the $TbPc_2$ layer. Such shift is significant considering the small amount of material deposited on the disks. This is due to the fact that $TbPc_2$ and the gold nanoantennas have slightly detuned optical resonances. In particular, LSPR is slightly redshifted with respect to the Q band of $TbPc_2$, thus falling at the maximum of the real part ε_1 of the dielectric function of the molecules (Figure S3, ESI; dielectric function of $TbPc_2$ evaporated on glass from Robaschik et al.[31]). This results in a strong LSPR shift, as reported and qualitatively explained by Haes et al. for a similar system.[50]

MCD spectra of **AuDisks**, **$TbPc_2$@Au** and **$TbPc_2$** were acquired at 1.5 K under a static magnetic field of 5 T. In a MCD experiment, the differential extinction $\Delta\zeta(\hbar\omega, B) = \zeta_-(\hbar\omega, B) - \zeta_+(\hbar\omega, B)$. between left and right circularly polarized light is acquired as a function of photon energy $\hbar\omega$ or static magnetic field B, applied parallel to the light propagation direction. The use of circularly polarized light introduces an additional selection rule for electronic transitions ($\Delta m_l = \pm 1$) that allows probing field-split orbitals and bands[51, 52]. Non-magnetic plasmonic nanoantennas exhibit distinct magneto-optical activity,[53-56] (Figure 3) which is shown in Figure 3a and should be taken into account in the molecular-nanoantenna system. The MCD response of **AuDisks** is a derivative-like line shape with respect to the optical resonance and arises from the magnetic field-induced modification of the circular plasmonic modes.[55, 57] When LSPR is excited by the circularly polarized light used in the MCD measurements, the resulting oscillation of free electrons follows circular orbits, which in turn are perturbed by the magnetic field that is applied perpendicular to their motion. This additional component of the Lorentz force is responsible for the spectral shift of the resonance. The sign of this shift depends on the direction of the applied magnetic field and on the helicity of the incoming light: in a typical MCD experiment the magnetic field is fixed, and light polarization is modulated between the left and right helicities, resulting in a higher and lower resonant energy with respect to the zero-field case, respectively. The difference between these two shifted spectra is shown in Figure 3a. Procedures for fitting the optical and MCD spectra of **AuDisks** are reported in the ESI and results can be found in Figure S4.

In **$TbPc_2$@Au** (Figure 3b) the MCD spectrum shows a more complex line shape, which can be disentangled into a derivative-shaped component crossing zero at 1.73 eV (Figure 3b, orange), related to the MCD response of the nanoantennas, and another peaking at 1.88 eV due to $TbPc_2$. The magneto-optical (MO) response of the $TbPc_2$ layer (Figure 3c) shows a main feature corresponding to the Q-band in the extinction spectrum.

To isolate the molecular contribution to the complex MCD line shape of the **$TbPc_2$@Au** spectrum, we consider that MCD is a differential extinction spectroscopic method. Therefore, assumptions that hold for extinction spectrum are also valid for MCD. In particular, we can consider the contributions to the MCD line shape arising from the plasmonic nanoantenna and from **$TbPc_2$** as additive. We can then subtract a calculated spectrum of the nanoantenna from the experimental data. To accurately reproduce the MCD contribution we fitted the low energy section of the MCD spectrum, in which the LSPR component is dominant, with the difference of two spectrally-shifted equal Lorentzian line shapes whose parameters were taken

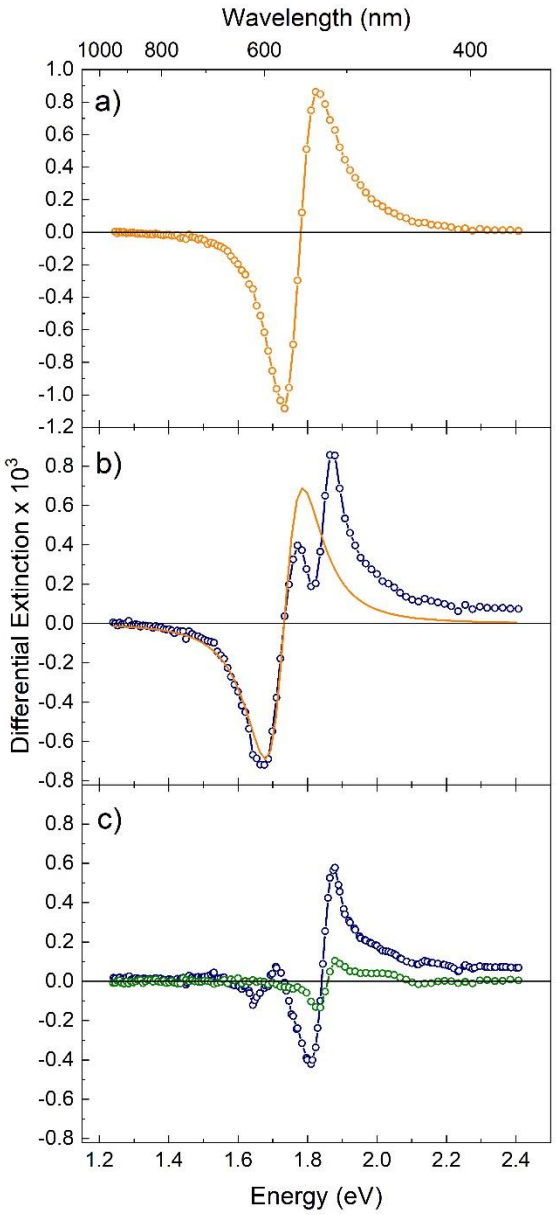

Figure 3. a) MCD spectrum of **AuDisks**; **b)** Raw MCD spectrum of **TbPc2@Au** (blue) with the estimated nanoantennas contribution (orange); **c)** Molecular part of the MCD spectrum of **$TbPc_2$@Au** corrected for the nanoantennas contribution (blue) and compared to the control MCD spectrum of **$TbPc_2$** (green). Spectra are plotted in differential extinction units (i.e. dichroism).

by the fitted extinction spectrum (Figure S4b). The contribution from the nanoantennas was then extrapolated to the high energy range of the MCD spectrum and subtracted from the experimental data, yielding the MCD contribution of the $TbPc_2$ layer in the composite structure reported in Figure 3 and compared to the same deposit on glass.

A qualitative comparison between optical and magneto-optical spectra of **Au@$TbPc_2$** suggests that plasmon-mediated enhancement of the molecular signal is of the same order of magnitude, and that the two enhancements share a common origin. This seems indeed to be the case, as shown by the following simple reasoning. Let us define the optical enhancement factor in a Surface Enhanced Absorption process[58] as a proportionality constant α between extinction ζ from the molecule and the enhanced extinction ζ_e of the same material over plasmonic nanoantennas: $\zeta_e = \alpha\zeta$. In MCD, the differential extinction $\Delta\zeta = \zeta_- - \zeta_+$ is measured, where $\zeta\pm$ is the absorption of left and right circularly polarized light, respectively. From this, it immediately follows that in a MCD experiment the enhancement factor α is directly carried through the differential extinction ($\Delta\zeta_e = \alpha\Delta\zeta$), confirming that plasmon-mediated MCD enhancement is a direct consequence of effects taking place at the optical level.

We can evaluate the experimental optical enhancement factor by comparing the integral of the extinction peak for the molecule in samples **$TbPc_2$** and **Au@$TbPc_2$**, respectively. For the latter sample, we performed a deconvolution of the plasmonic and molecular components (as described in ESI and shown in Figure S5), then evaluated the integral of the molecular contribution. The ratio between integrals of the molecular components in **Au@TPc_2** and **$TbPc_2$** is 5.5. Since the two samples contain the same number of molecules per unit area, this ratio can be considered the plasmon-mediated enhancement factor α. As a further control experiment to point out the role of spectral overlap between optical resonances, we also evaporated a thin film of $TbPc_2$ on a second set of nanoantennas (R = 85 nm, h = 15 nm) the LSPR of which, at 1.44 eV, is almost fully detuned with respect to that of $TbPc_2$. Extinction spectra of this sample showed that the molecular component undergoes no significant enhancement of its intensity compared to the co-deposited layer of $TbPc_2$ on glass. LSPR position is also hardly affected (see Figure S6, ESI).

To evaluate the magneto-optical enhancement factor, the same procedure was carried out on the MCD spectra of **$TbPc_2$** and **Au@$TbPc_2$**. Since MCD is a signed quantity, the integral was calculated on the absolute value of the spectrum. The molecular component of **Au@$TbPc_2$** was extracted as described above and shown in Figure 3c. The ratio between integrals was found to be 4.8. The value is very close to the one found for the optical spectra, confirming that the enhancement factor α is transferred from the optical to the magneto-optical response, ultimately suggesting that magneto-optical plasmon enhancement originates from optical effects in the first place. This finding has a twofold relevance: i) it sheds light on the evanescent field of plasmon-enhanced magneto-optics, by clearly and reasonably finding the origin of such effect at the optical level; ii) it opens countless possibilities for the optimization of plasmon enhancement of magneto-optical effects, since the same ground rules for optical enhancement hold for magneto-optics.

Direct information on the magnetic behavior of the $TbPc_2$ thin film can be obtained from the magnetization curves, scanning the magnetic field at fixed photon energy and collecting the MCD. The linear field response of **AuDisks** at the positive lobe (E = 1.82 eV, Figure S7, ESI), originating from the mechanism described above, allows straightforward and precise correction of the plasmonic contribution to the magneto-optical signal, leaving full access to the properties of the molecular species. In Figure 4a we show the MCD hysteresis curve of **$TbPc_2$@Au** at the positive maximum (E = 1.87 eV). The contribution of nanoantennas to the MCD hysteresis loops of **$TbPc_2$@Au** can be easily calculated from the magnitude of the magneto-optical signal of the gold nanoantennas and taking advantage of its linear dependence on applied magnetic field it can

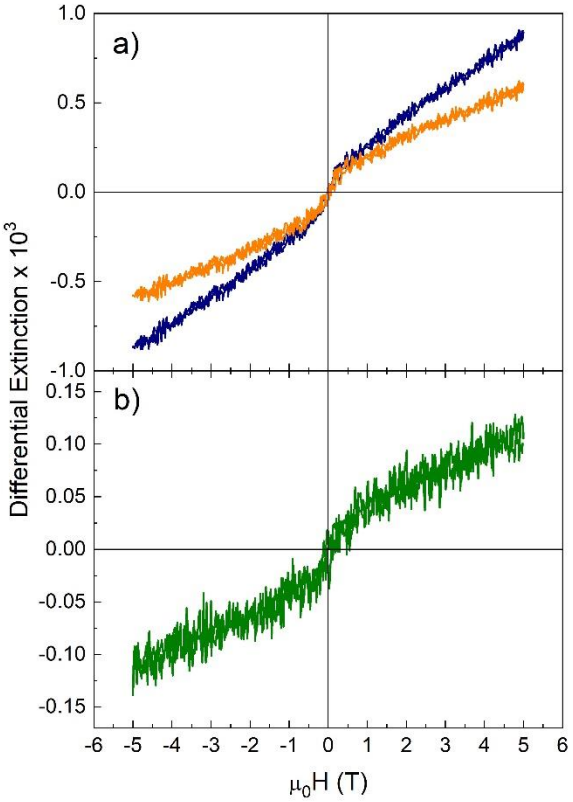

Figure 4. MCD hysteresis loops acquired at T = 1.5 K, field scan rate: 150 Oe.s^{-1}. **a) TbPc$_2$@Au** as acquired at the positive maximum of the MCD spectrum (E = 1.87 eV, blue) and after correction for the nanoantenna contribution (orange). **b) TbPc$_2$** acquired at the positive (blue) maximum of the Q band (E = 1.87 eV).

be precisely subtracted to isolate the hysteresis loop of the TbPc$_2$ film. For comparison, Figure 4b features the MCD hysteresis loop of **TbPc$_2$** taken at the same energy. As expected, the scaling between the two samples (5.4) agrees excellently with the estimated earlier enhancement by the nanoantennas.

The shape of the corrected MCD loop for **TbPc$_2$@Au** shows a non-saturating behavior, and the absence of hysteresis opening. The same can be observed, but with higher noise, for **TbPc$_2$**. This is likely related to the orientation of the TbPc$_2$ molecules in the composite architecture. Standing-up assembly on glass substrates has been reported for TbPc2, while the latter is known to organize in lying-down configuration on clean gold surface although this arrangement converts to the standing configuration for a thickness of few nm, both at room[38] and low temperature.[37,46]

Here, with Au nanoantennas the metallic surface is not atomically clean/flat and it is reasonable to assume that molecules assemble in standing-up position like on the rest of the substrate. This arrangement results in a perpendicular orientation of the molecule's easy axis of magnetization with respect to the applied magnetic field, so saturation is not reached at the maximum applied field, while the small, rapid increase of magnetization observed at weak fields could be attributed to minor deviations from a perfect standing molecular configuration. On the other hand, hysteresis opening is not expected for this molecular orientation due to the mixing of spin states of opposite sign by magnetic field components which are transverse with respect to the easy axis. With this molecular arrangement, a 2 nm deposit can be limited roughly to two monolayers of TbPc$_2$.

Conclusions

In summary, we reported the first observation of plasmon-enhanced magneto-optics in a system made up of a single-molecule magnet thin film on a nanoantenna array. By using a weak molecule-nanoantenna coupling model, we demonstrate a fivefold optical enhancement. The enhancement afforded by the nanoantennas in this report currently allows studying down to two molecular monolayers with spectroscopic and magnetometric degrees of freedom. Considering the noise level of the MCD setup used, sub-monolayers of magnetic molecules on surfaces can in principle be detected (see quantitative estimates in ESI). At the same time, the distinct magneto-optical response of molecules and nanoantennas allows for precise subtraction of the plasmonic contribution to the MCD signal. With further optimization of the nanoantennas and of molecule deposition methods it should be possible to achieve strong magneto-optics enhancement, giving access to routine investigations in the sub-monolayer regime, currently challenging even for the cutting edge synchrotron-based X-ray magnetic spectroscopy methods.[31,32,49] This could give a tremendous boost to the design and fabrication of readout-enabled molecule-based magnetic devices.

In addition, we made a strong correlation between optical and magneto-optical plasmon enhancement factors, which we found to be very similar experimentally and conceptually identical, suggesting that the origin of magneto-optical enhancement can be fully explained on the basis of optical enhancement. It is reasonable to assume that this behavior is general (i.e. not restricted to magnetic molecules on gold disks); hence, we conclude suggesting that design rules to achieve extreme plasmon-enhanced magneto-optics could be adopted from the extensive pool of knowledge of other plasmon-enhanced spectroscopies.

Methods

Fabrication of Au nanodisks: Short-range ordered arrays of plasmonic Au nanodisks were prepared using hole-mask colloidal lithography.[38] The diameters of polystyrene beads define the size of the corresponding nanodisks via normal metal deposition with e-beam evaporation. The diameter of the nanodisks is 125 nm with the height of 35 nm. All antennas are produced on 0.4 mm-thick square (1.5 x 1.5 cm) Menzel-Gläser glass. The structure and morphology of the plasmonic nanoantennas were investigated using Scanning Electron Microscopy (SEM) for general morphology and lateral size (Figure 1) and Atomic Force Microscopy (AFM) for thickness (data not shown).

Synthesis of TbPc$_2$: Microcrystalline powders of the neutral Tb(III) bis-phthalocyaninato complex were prepared following the procedure by De Cian et al.[33]

Preparation of TbPc$_2$ thin films: Glass substrates were cleaned by sonication for 10 minutes in acetone, followed by isopropanol and dried in a flow of nitrogen. Plasmonic substrates were used without further treatment. Deposition of the TbPc$_2$ layers was carried out by sublimation using a home-built Knudsen cell, using powders that were degassed for several days before sample preparation. The base pressure during the sublimation was <10^{-6} mbar and the deposition

rate was ≈0.2 Å/min, as measured by quartz crystal microbalance before exposing the substrates. The effective thickness of the deposits on Au disks and on glass was estimated by comparing the integral of the $TbPc_2$ extinction Q band at 1.85 eV against an extinction vs thickness calibration curve on thicker $TbPc_2$ deposits on glass (see Figure S8 for details). The thickness of the calibration deposits was verified by scratching the film with a needle and measuring the depth of the scratch with a NT-MDT P47-PRO atomic force microscope (NT-MDT, Zelenograd Russia). Sample morphology after deposition and homogeneity of the molecular layer was checked with AFM (see Figure S9).

Optical and magneto-optical spectra: Extinction measurements were carried out on a Jasco V-660 spectrophotometer (Jasco Corporation, Tokyo Japan) in transmission mode. Magnetic-circular dichroism experiments were carried out on a home-build setup. Briefly, light emitted by a Xe-Hg arc lamp is monochromated and polarized linearly. Light then passes through a photoelastic modulator which alternates polarization between left and right circular states at approximately 50 kHz. The beam then travels through the sample, placed in an optical cryostat equipped with a superconducting magnet. Applied magnetic field is collinear with the light propagation direction. Light is recovered with a silicon photodiode, and the magneto-optical signal is computed as the ratio between the component of the photodiode output at the polarization modulation frequency (recovered with a lock-in amplifier) and the static output of the diode. MCD spectra are acquired by scanning the photon energy with fixed magnetic field, while MCD hysteresis loops are recorded by scanning the magnetic field magnitude at fixed photon energy.

Conflicts of interest

There are no conflicts to declare.

Author contributions

FP, GC and MM conceived the experiment; MS, LP and AM prepared and characterized the samples; FP, GC and VB performed the MCD experiment; EPV and ES performed numerical simulations; FP, MG and RS interpreted data; all authors contributed to the writing of the manuscript.

Acknowledgement

This work has been supported by the European Union's Horizon2020 Research and Innovation program under Grant agreement No. 737709 (FEMTOTERABYTE http://www.physics.gu.se/femtoterabyte), by MIUR through the FIRB project "NanoPlasMag" (RBFR10OAI0) and by the University of Pisa through project PRA_2017_25. The simulations were performed on resources at Chalmers Centre for Computational Science and Engineering (C3SE) provided by the Swedish National Infrastructure for Computing (SNIC) (SNIC2018-4-38). B. Cortigiani and D. Rovai are fully acknowledged for their technical support during the preparation of the samples.

Notes and references

1. H. A. Atwater, *Scientific American*, 2007, **296**, 56-62.
2. U. Kreibig and M. Vollmer, *Optical properties of metal clusters*, Springer, Berlin, 1995
3. C. F. Bohren and D. R. Huffman, *Absorption and scattering of light by small particles*, John Wiley & Sons, 2008.
4. S. A. Maier, *Plasmonics - Fundamentals and Applications*, Springer, New York, 2007.
5. T. Grosjean, M. Mivelle, F. Baida, G. Burr and U. Fischer, *Nano letters*, 2011, **11**, 1009-1013.
6. M. D. Sonntag, J. M. Klingsporn, A. B. Zrimsek, B. Sharma, L. K. Ruvuna and R. P. Van Duyne, *Chemical Society reviews*, 2014, **43**, 1230-1247.
7. K. Aslan, I. Gryczynski, J. Malicka, E. Matveeva, J. R. Lakowicz and C. D. Geddes, *Current Opinion in Biotechnology*, 2005, **16**, 55-62.
8. W. Johnson, S. Kim, Z. Utegulov, J. Shaw and B. Draine, *The Journal of Physical Chemistry C*, 2009, **113**, 14651-14657.
9. I. Lieberman, G. Shemer, T. Fried, E. M. Kosower and G. Markovich, *Angewandte Chemie International Edition*, 2008, **47**, 4855-4857.
10. L. Wang, C. Clavero, Z. Huba, K. J. Carroll, E. E. Carpenter, D. Gu and R. A. Lukaszew, *Nano Letters*, 2011, **11**, 1237-1240.
11. S. Tomita, K. Takeshi, T. Shigeru, I. Satoshi, F. Minoru and H. Shinji, *Physical Review Letters*, 2006, **96**, 167402.
12. D. Meneses-Rodríguez, E. Ferreiro-Vila, P. Prieto, J. Anguita, M. U. González, J. M. García-Martín, A. Cebollada, A. García-Martín and G. Armelles, *small*, 2011, **7**, 3317-3323.
13. P. K. Jain, Y. Xiao, R. Walsworth and A. E. Cohen, *Nano Letters*, 2009, **9**, 1644-1650.
14. D. Melnikau, A. A. Govyadinov, A. Sánchez-Iglesias, M. Grzelczak, L. M. Liz-Marzán and Y. P. J. N. l. Rakovich, *Nano letters*, 2017, **17**, 1808-1813.
15. D. Bossini, V. Belotelov, A. Zvezdin, A. Kalish and A. Kimel, *Acs Photonics*, 2016, **3**, 1385-1400.
16. D. Ellsworth, L. Lu, J. Lan, H. Chang, P. Li, Z. Wang, J. Hu, B. Johnson, Y. Bian and J. Xiao, *Nature Physics*, 2016, **12**, 861-866.
17. D. Gatteschi, R. Sessoli and J. Villain, *Molecular nanomagnets*, OUP Oxford, 2006.
18. L. Thomas, F. Lionti, R. Ballou, D. Gatteschi, R. Sessoli and B. Barbara, *Nature*, 1996, **383**, 145-147.
19. E. Moreno-Pineda, C. Godfrin, F. Balestro, W. Wernsdorfer and M. Ruben, *Chemical Society Reviews*, 2018, **47**, 501-513.
20. A. R. Rocha, V. M. Garcia-Suarez, S. W. Bailey, C. J. Lambert, J. Ferrer and S. Sanvito, *Nature materials*, 2005, **4**, 335.
21. S. Sanvito, *Chemical Society Reviews*, 2011, **40**, 3336-3355.
22. M. Cinchetti, *Nature nanotechnology*, 2014, **9**, 965-966.
23. G. Cucinotta, L. Poggini, A. Pedrini, F. Bertani, N. Cristiani, M. Torelli, P. Graziosi, I. Cimatti, B. Cortigiani and E. Otero, *Advanced Functional Materials*, 2017, **27**, 1703600.
24. C. Wäckerlin, F. Donati, A. Singha, R. Baltic, S. Rusponi, K. Diller, F. Patthey, M. Pivetta, Y. Lan and S. Klyatskaya, *Advanced Materials*, 2016, **28**, 5195-5199.
25. A. Cornia, M. Mannini, P. Sainctavit and R. Sessoli, *Chemical Society Reviews*, 2011, **40**, 3076-3091.
26. M. Mannini, F. Pineider, C. Danieli, F. Totti, L. Sorace, P. Sainctavit, M. A. Arrio, E. Otero, L. Joly, J. C. Cezar, A. Cornia and R. Sessoli, *Nature*, 2010, **468**, 417-421.
27. M. Mannini, F. Pineider, P. Sainctavit, C. Danieli, E. Otero, C. Sciancalepore, A. M. Talarico, M. A. Arrio, A. Cornia, D. Gatteschi and R. Sessoli, *Nat Mater*, 2009, **8**, 194-197.

28. L. Malavolti, V. Lanzilotto, S. Ninova, L. Poggini, I. Cimatti, B. Cortigiani, L. Margheriti, D. Chiappe, E. Otero and P. Sainctavit, *Nano letters*, 2015, **15,** 535-541.
29. N. Ishikawa, M. Sugita, T. Ishikawa, S.-y. Koshihara and Y. Kaizu, *Journal of the American Chemical Society*, 2003, **125**, 8694-8695.
30. L. Margheriti, D. Chiappe, M. Mannini, P. E. Car, P. Sainctavit, M. A. Arrio, F. B. de Mongeot, J. C. Cezar, F. M. Piras and A. Magnani, *Advanced Materials*, 2010, **22**, 5488-5493.
31. P. Robaschik, M. Fronk, M. Toader, S. Klyatskaya, F. Ganss, P. F. Siles, O. G. Schmidt, M. Albrecht, M. Hietschold and M. Ruben, *Journal of Materials Chemistry C*, 2015, **3**, 8039-8049.
32. M. Serri, M. Mannini, L. Poggini, E. Vélez-Fort, B. Cortigiani, P. Sainctavit, D. Rovai, A. Caneschi and R. Sessoli, *Nano letters*, 2017, **17**, 1899-1905.
33. A. De Cian, M. Moussavi, J. Fischer and R. Weiss, *Inorganic chemistry*, 1985, **24**, 3162-3167.
34. K. Kizaki, H. Ozawa, T. Kobayashi, R. Matsuoka, Y. Sakaguchi, A. Fuyuhiro, T. Fukuda and N. Ishikawa, *Chemical Communications*, 2017, **53**, 6168-6171.
35. M. Gonidec, E. S. Davies, J. McMaster, D. B. Amabilino and J. Veciana, *Journal of the American Chemical Society*, 2010, **132**, 1756-1757.
36. L. Malavolti, M. Mannini, P.-E. Car, G. Campo, F. Pineider and R. Sessoli, *Journal of Materials Chemistry C*, 2013, **1**, 2935-2942.
37. P. Robaschik, P. F. Siles, D. Bülz, P. Richter, M. Monecke, M. Fronk, S. Klyatskaya, D. Grimm, O. G. Schmidt and M. Ruben, *Beilstein journal of nanotechnology*, 2014, **5**, 2070-2078.
38. H. Fredriksson, Y. Alaverdyan, A. Dmitriev, C. Langhammer, D. S. Sutherland, M. Zäch and B. Kasemo, *Advanced Materials*, 2007, **19**, 4297-4302.
39. M. Perfetti, M. Serri, L. Poggini, M. Mannini, D. Rovai, P. Sainctavit, S. Heutz and R. Sessoli, *Advanced Materials*, 2016, **28**, 6946-6951.
40. J. Mack, M. J. Stillman and N. Kobayashi, *Coordination chemistry reviews*, 2007, **251**, 429-453.
41. G. A. Wurtz, P. R. Evans, W. Hendren, R. Atkinson, W. Dickson, R. J. Pollard, A. V. Zayats, W. Harrison and C. Bower, *Nano letters*, 2007, **7**, 1297-1303.
42. N. T. Fofang, T.-H. Park, O. Neumann, N. A. Mirin, P. Nordlander and N. J. Halas, *Nano letters*, 2008, **8**, 3481-3487.
43. A. De Luca, R. Dhama, A. Rashed, C. Coutant, S. Ravaine, P. Barois, M. Infusino and G. Strangi, *Applied Physics Letters*, 2014, **104**, 103103.
44. D. Melnikau, R. Esteban, D. Savateeva, A. Sánchez-Iglesias, M. Grzelczak, M. K. Schmidt, L. M. Liz-Marzán, J. Aizpurua and Y. P. Rakovich, *The Journal of Physical Chemistry Letters*, 2016, **7**, 354-362.
45. N. T. Fofang, N. K. Grady, Z. Fan, A. O. Govorov and N. J. Halas, *Nano letters*, 2011, **11**, 1556-1560.
46. A. Manjavacas, F. G. a. d. Abajo and P. Nordlander, *Nano letters*, 2011, **11**, 2318-2323.
47. R. D. Artuso and G. W. Bryant, *Nano letters*, 2008, **8**, 2106-2111.
48. B. Peng, Ş. K. Özdemir, W. Chen, F. Nori and L. Yang, *Nature Communications*, 2014, **5**, 5082.
49. N. Caselli, F. Intonti, F. La China, F. Biccari, F. Riboli, A. Gerardino, L. Li, E. H. Linfield, F. Pagliano and A. Fiore, *Nature Communications*, 2018, **9**, 396.
50. A. J. Haes, S. Zou, J. Zhao, G. C. Schatz and R. P. Van Duyne, *Journal of the American Chemical Society*, 2006, **128**, 10905-10914.
51. W. R. Mason, *A practical guide to magnetic circular dichroism spectroscopy*, Wiley-Interscience, New York, 2007.
52. F. Pineider and C. Sangregorio, in *Magnetic Characterization Techniques for Nanomaterials*, Springer, 2017, pp. 457-509.
53. M. A. Zaitoun, W. R. Mason and C. T. Lin, *The Journal of Physical Chemistry B*, 2001, **105**, 6780-6784.
54. B. Sepúlveda, J. B. González-Díaz, A. García-Martín, L. M. Lechuga and G. Armelles, *Physical Review Letters*, 2010, **104**, 147401.
55. F. Pineider, G. Campo, V. Bonanni, J. Fernandez Cde, G. Mattei, A. Caneschi, D. Gatteschi and C. Sangregorio, *Nano Letters*, 2013, **13**, 4785-4789.
56. B. Han, X. Gao, L. Shi, Y. Zheng, K. Hou, J. Lv, J. Guo, W. Zhang and Z. J. N. l. Tang, 2017, **17**, 6083-6089.
57. G. Weick and D. Weinmann, *Physical Review B*, 2011, **83**, 125405.
58. T. Itoh, Y. S. Yamamoto and Y. Ozaki, *Chemical Society reviews*, 2017, **46**, 3904-3921.